

A PERFORMANCE STUDY OF A
PULSED SOLID FUEL MICROTHRUSTER

by

ROGER JAMES RADLEY, JR.

S.B., Massachusetts Institute of Technology

(1968)

SUBMITTED IN PARTIAL FULFILLMENT

OF THE REQUIREMENTS FOR THE

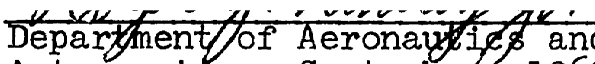
DEGREE OF MASTER OF SCIENCE

at the

MASSACHUSETTS INSTITUTE OF TECHNOLOGY

September, 1969

Signature of Author


Department of Aeronautics and
Astronautics, September, 1969

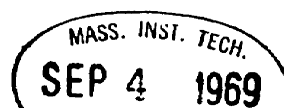
Certified by _____

Thesis Supervisor

Accepted by _____

Chairman, Departmental
Graduate Committee

Archives



A PERFORMANCE STUDY OF A
PULSED SOLID FUEL MICROTHRUSTER

by

Roger James Radley, Jr.

Submitted to the Department of Aeronautics and
Astronautics on August 18, 1969, in partial fulfillment
of the requirements for the degree of Master of Science.

ABSTRACT

In this thesis, ways of improving the performance of the LES-6 pulsed solid fuel microthruster are investigated. To measure the impulse bit, a thrust balance was constructed utilizing a pendulum mounted in an evacuated bell jar. The mass expended during each run was measured to compute specific impulse and efficiency. These three quantities were measured with less than a 3% error.

The methods of improvement concentrated upon were designed to increase performance by increasing the self-induced magnetic field. This was accomplished by using a yoke, and by changing the current path using loops of wires next to the sides of the thrust chambers. In the best configuration, the specific impulse was increased from 348 to 1002 seconds, the impulse bit being decreased from 6.83 to 2.11 μ lb-sec. and efficiency from 2.8% to 2.5%.

Thesis Supervisor: Albert Solbes

Title: Associate Professor of
Aeronautics and Astronautics

ACKNOWLEDGEMENTS

The author wishes to express his deepest appreciation to Professor Solbès who devoted so much time and effort to this thesis. The author also thanks Fred Merlis and John Stevens for their hours of help in designing and building the experimental apparatus. Finally, acknowledgement is made to Robert Vondra and the people at the Lincoln Laboratory who funded the project under DSR 71382 and supplied LES-6 microthrusters tested.

TABLE OF CONTENTS

<u>Chapter No.</u>		<u>Page No.</u>
1	Introduction	9
2	Thruster	10
3	Thrust Balance	19
4	Experiments	40
5	Conclusion	55
<u>Appendix</u>	Error Analysis	56
<u>References</u>		61

LIST OF FIGURES

<u>Figure No.</u>		<u>Page No.</u>
1	Circuit Diagram of LES-6 Microthruster	11
2	Schematic Side View of Main Capacitor Circuit	13
3	Photograph of Experimental Apparatus	20
4	Photograph of Pendulum, Support Stand, and Laser	21
5	Scale Drawing of Pendulum (Rear View)	22
6	Triggering Circuit Diagram	27
7	Meter Stick Reading Versus Time for Run #28	35
8	Plot of α_N Versus Time for Damping Data of Run #23	36
9	α_∞ Versus Time for Run #23	38
10	Schematic Top Views of the Two Thrust Chambers with Various Current Loop Configurations	41
11	Thruster Performance for Various Current Loop Configurations	51

NOTATION

A = constant in the formula for impulse bit

$$= mg \frac{l}{l'} \frac{T^2}{2\pi}$$

C = capacitance of main capacitor

c = average speed of gas molecules

E = total energy stored in main capacitor = $\frac{1}{2}CV^2$

f = frequency of pendulum

g = acceleration due to gravity = 9.81 m/s²

I = impulse bit of the thruster

I_{sp} = specific impulse

i = current in main capacitor circuit

L = total inductance of main capacitor circuit

L' = dimensionless inductance ratio = (L₀ + L₁)/L₀

L₀ = inductance of original thruster configuration

L₁ = additional inductance due to modifications

$\langle dL/dx \rangle$ = average change of circuit inductance with
respect to the coordinate x

l = characteristic length (as used in Chapter 2)

l = distance from axis of rotation to center of
mass of the pendulum (as used in Chapter 3
and Appendix)

l' = distance from axis of rotation to center of
thrust of pendulum

m = mass of pendulum

- m = mass of pendulum
- m_s = mass of the slug of teflon ablated in each shot
- Δm = mass of teflon expended during an experimental run
- N = number of gas molecules impinging on the face of a fuel element between pulses (as used in Chapter 3, Section D).
- N = total number of thruster pulses fired during a run (as used in Chapter 3, Sections E and F, and Appendix)
- n_{gas} = number of gas molecules in electrode gap between shots
- n_{teflon} = number of teflon molecules ablated per shot
- R = total resistance of main capacitor circuit
- $\langle R \rangle$ = average circuit resistance
- R_m = magnetic Reynolds number
- S = surface area of the face of a fuel element (as used in Chapter 3, Section D).
- S = slope of α_N versus t curve for direct fire (as used in Chapter 3, Section F).
- S' = slope of α_N versus t curve for retro fire
- t = time
- T = period of pendulum
- Δt_f = total firing time during a run
- u = velocity of plasma (discharge)

u_f = final (exhaust) velocity of plasma

u_i = initial plasma velocity = 0

V = voltage of main capacitor

X = coordinate along the electrode which
characterizes the position of the discharge

α = deflection angle (in radians) of pendulum
from rest position

α_f = angle at which thruster stops firing near
the bottom of the pendulum's swing

α_i = angle at which thruster starts firing near
the bottom of the pendulum's swing

α_N = pendulum deflection angle which is a function
of time

α_{N_0} = deflection angle for zero thrust = $\alpha_0 e^{-\nu t}$

α_0 = initial deflection angle of pendulum

α'_0 = deflection angle at the start of retro firing

η = thruster efficiency

μ = magnetic permeability (Note: When used as a
prefix to units, μ means micro- and equals
 10^{-6})

$1/\nu$ = damping time of pendulum

σ = conductivity of the plasma

ω = angular frequency of pendulum = $2\pi/T$

$\omega_c = \omega / (1 - \nu^2/\omega^2)$

1. Introduction

Electric propulsion has been shown to be superior to more conventional acceleration systems for certain space missions because of its high exhaust velocities. This feature results in more efficient use of the propellant and hence makes possible a larger payload for a given initial vehicle mass. Successful electric thrusters have been built and tested, and could be useful for high specific impulse space missions provided a high power density energy source can be built.

Pulsed solid propellant thrusters have a number of advantages over chemical thrusters and other types of propulsion. The first is that of simplicity. There are no valves or moving parts, and there is no need for pressurized fuel tanks for zero-gravity environments. These thrusters require no warm-up time and can be easily and precisely controlled. They have a lifetime of several million pulses and simply no longer fire when failure occurs. Chemical thrusters do not have this fail-safe mode. Finally, with the use of a power conditioning unit, the low voltage output of solar batteries is sufficient for operation.

These features make a pulsed solid fuel microthruster ideal for station keeping of synchronous satellites and justify a more intensive investigation to improve *its* performance.

2. Thruster

A. Generalities

The thruster under study is the LES-6 pulsed solid fuel microthruster which was built for the M.I.T. Lincoln Laboratory by Fairchild Hiller.¹ The unit is approximately 7 inches long, 6 inches high, and 3-3/4 inches wide and weighs about 3 pounds. It has two thrust chambers arranged side by side, each consisting of 2 electrodes, 1 spark plug, and the rectangular face of a spring-fed teflon fuel element. This microthruster provides an impulsive thrust of about 3 microseconds duration and can be pulsed as often as 10 times a second for several million times. It has an impulse bit of 6 to 7 micropound-seconds and a specific impulse of 270 to 350 seconds. Although the LES-6 is a prototype for larger microthrusters, it is presently being used in earth orbit on a Lincoln Lab experimental satellite (LES).

The thruster operates by the gasdynamic and electromagnetic acceleration of ablated teflon. This is accomplished by the discharge of 1.85 joules of energy, stored in the main capacitor (charged to 1360 volts), across the face of one of the teflon fuel elements. The main discharge is initiated by a 6-volt pulse which triggers the discharge of a 500-volt capacitor across the spark plug gap (see Figure 1 for the thruster circuit diagram). The spark plug firing in the inter-electrode gap initiates the breakdown at only 1360 volts.

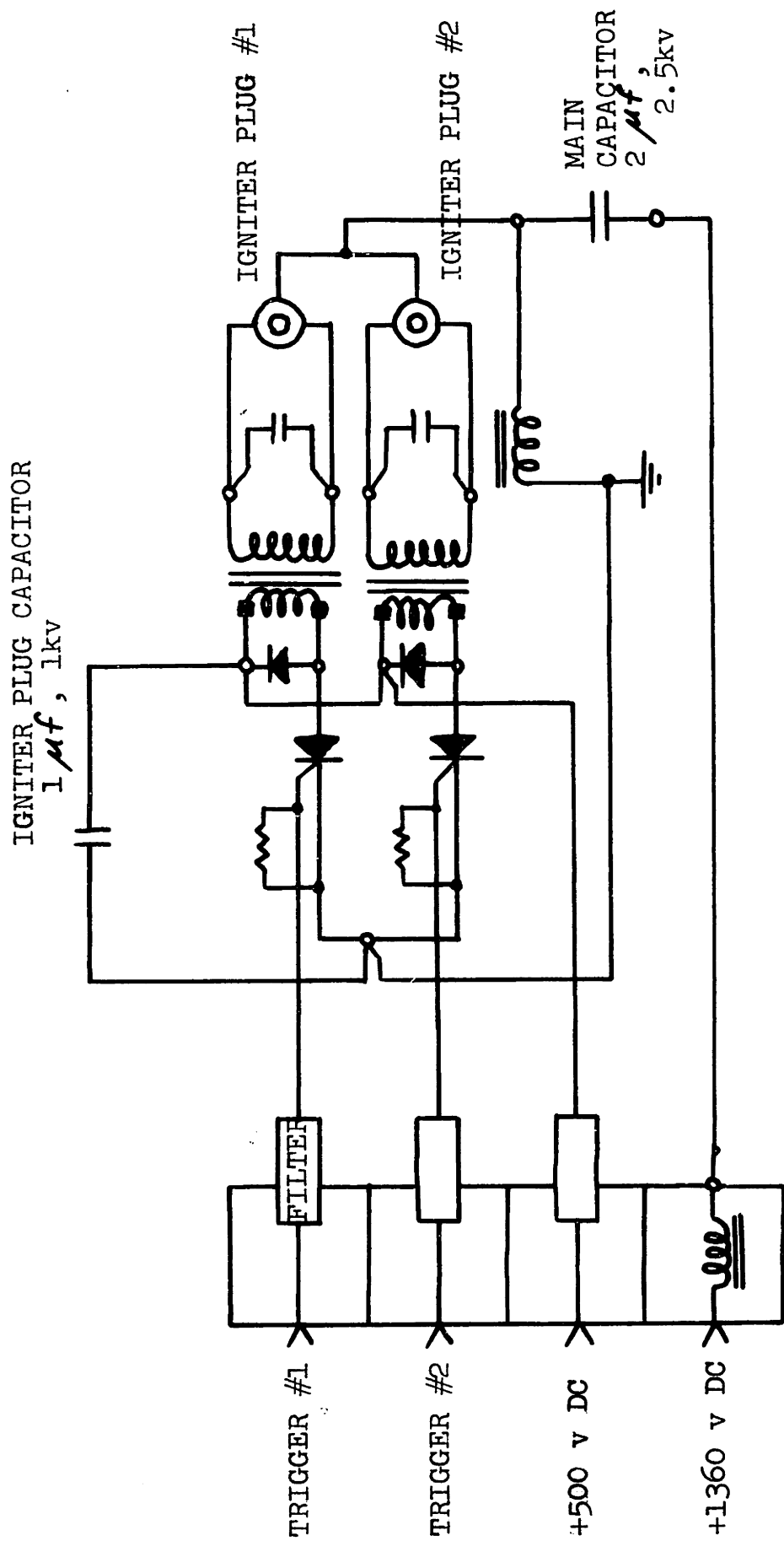


Figure 1. CIRCUIT DIAGRAM OF LES-6 MICROTHRUSTER

The 1.85 joules of total energy in the main capacitor ablates off about 10^{-5} grams of teflon per shot from the 3 cm by 1 cm rectangular face of the fuel element, breaks up the molecules, ionizes the atoms, heats the electrons to a high temperature, and accelerates the gas out of the thrust chamber. A significant part of the thrust (perhaps as high as 50%) is probably due to the thermal expansion of the hot gas. The rest is due to the self-induced magnetic field (i.e., the $\vec{j} \times \vec{B}$ force on the plasma). Hence, as much as 150 seconds of the specific impulse may be the result of gas-dynamic acceleration of the exhaust gases.

B. Slug Model

One model which can be used to describe the thruster performance mathematically is the slug model. This model is based on the assumption that the ablated teflon is a slug of gas travelling at the same velocity as the main electrical discharge.

The main capacitor circuit equation can be written in the following way:

$$V = Ri + \frac{d}{dt} (Li)$$

V is the capacitor voltage, i the current, L the total inductance, and R the total resistance. A schematic side view of this circuit is shown in Figure 2. In order to account for any possible modifications (see Chapter 4), L must include the additional inductance. In general, $L = L_0 + L_1$ where L_0 is

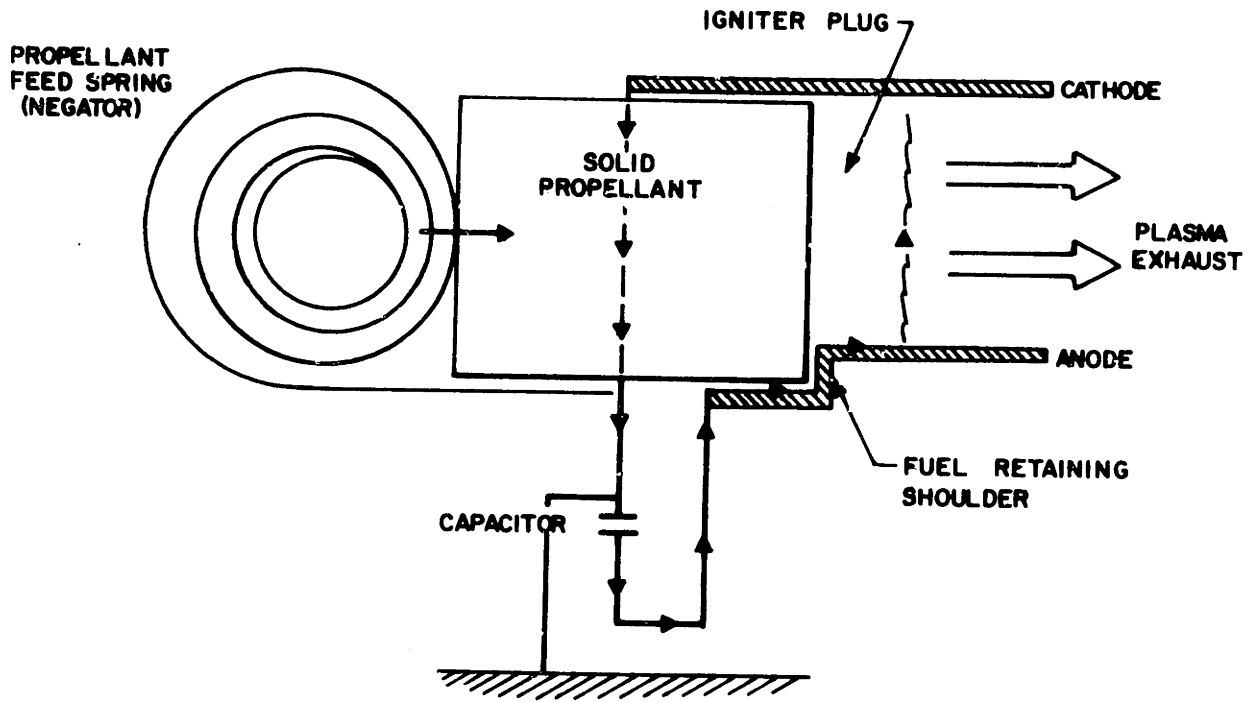


FIGURE 2. SCHEMATIC SIDE VIEW OF MAIN CAPACITOR CIRCUIT¹

the inductance of the original circuit and L_1 is the inductance change due to any modifications. The resistance R is the sum of the resistance of the main capacitor and of the plasma.

Multiplying both sides of the circuit equation by i and integrating over time for one pulse gives the following:

$$\int_0^{\infty} V i dt = E = \int_0^{\infty} R i^2 dt + \left[\frac{1}{2} L i \right]_{t=0}^{\infty} + \int_0^{\infty} \frac{1}{2} i^2 \frac{dL}{dt} dt$$

The first term on the right-hand side is the power dissipated in the circuit resistance. The second term is zero because the current i equals zero at $t = 0$ and $t = \infty$. The last term is the work done by the $\vec{j} \times \vec{B}$ force on the plasma. It will eventually be desirable to increase this last term. The slug model implies that $\frac{dx}{dt} = u$, u being the velocity of the plasma and x being a coordinate which characterizes the position of the discharge. The efficiency η can be defined as

$$\eta = \frac{\int_0^{\infty} \frac{1}{2} i^2 \frac{dL}{dx} \frac{dx}{dt} dt}{E} = \frac{1}{E} \int_0^{\infty} \frac{1}{2} i^2 u \frac{dL}{dx} dt$$

For the normal configuration of the thruster, dL/dx is nearly constant and depends on electrode geometry. Also

$$u \Big|_0^{\infty} = \frac{u_f - u_i}{2} = \frac{u_f}{2}$$

where u_f = the final velocity of the plasma, so that

$$\eta \approx \frac{1}{2} \frac{dL}{dx} \frac{u_f}{2} \int_0^{\infty} i^2 dt$$

An average resistance $\langle R \rangle$ may be defined as follows:

$$\langle R \rangle = \frac{\int_0^{\infty} R i^2 dt}{\int_0^{\infty} i^2 dt}$$

Using the above definitions, the expression for the energy E stored in the main capacitor becomes

$$E = \frac{\langle R \rangle \int_0^{\infty} L^2 dt}{1 - \eta}$$

Solving for η and eliminating E gives the first important equation:

$$\frac{\eta}{1 - \eta} = \frac{1}{4} \frac{\langle dL/dx \rangle}{\langle R \rangle} u_f \quad (2-1)$$

Another expression for $\eta/1 - \eta$ can be written by noting that resistance $R = \frac{1}{\sigma} \frac{l}{S} \sim \frac{1}{\sigma l}$ where σ is the conductivity of the plasma and l is a characteristic length. The quantity dL/dx is on the order of μ , the magnetic permeability of vacuum. These two approximations put into equation 2-1 give the following result:

$$\frac{\eta}{1 - \eta} \sim \frac{1}{4} \mu \sigma l u_f = \frac{R_m}{4} \quad (2-2)$$

R_m is the magnetic Reynold's number characterizing the thruster. The order of magnitude of η and R_m will be examined in the next section.

An alternative definition of efficiency is the following:

$$\eta = \frac{\text{kinetic energy of exhaust}}{\text{total energy}} = \frac{m_s u_f^2 / 2}{E}$$

where m_s is the mass of the slug of ablated teflon. But the impulse bit I is equal to $m_s u_f$ and the specific impulse I_{sp}

is u_f/g so that equation for η can be rewritten

$$\eta = \frac{I u_f/2}{E} \quad (2-3a)$$

or

$$\eta = \frac{g}{2} \frac{I I_{sp}}{E} \quad (2-3b)$$

Substitution of equation 2-3a into equation 2-1 gives an expression for I/E :

$$\frac{I}{E} = \frac{1-\eta}{2} \frac{\langle dL/dx \rangle}{\langle R \rangle} \quad (2-4)$$

Eliminating η from the above equation it is found that:

$$\frac{I}{E} = \frac{1}{2} \frac{\langle dL/dx \rangle / \langle R \rangle}{1 + \frac{1}{4} \frac{\langle dL/dx \rangle}{\langle R \rangle} u_f}$$

When $\langle dL/dx \rangle / \langle R \rangle \gg 1$, $I/E \cong 2/u_f$ or $E \cong \frac{m_p u_f^2}{2}$ and $\eta = 1$. This limit serves as a check on the above equation to insure that it provides a reasonable result when η is high. In reality, for the thruster under consideration, $\langle dL/dx \rangle / \langle R \rangle$ is much less than 1 which leads to the final expression for I/E :

$$\frac{I}{E} = \frac{1}{2} \frac{\langle dL/dx \rangle}{\langle R \rangle} \quad (2-5)$$

Therefore, to improve the impulse bit for a given energy level of this thruster it is necessary to increase $\langle dL/dx \rangle$ and decrease $\langle R \rangle$.

C. Performance and Possible Improvements

Some of the actual performance parameters of the LES-6

microthruster have been mentioned previously. The rest will be presented here.

The main capacitor has a capacitance of $2 \mu\text{f}$, and the electrode gap breaks down reliably at about 1360 volts so that the energy of the discharge is 1.85 joules. The total circuit inductance of the original configuration is about 4×10^{-8} henry. The total resistance of the main circuit is approximately 0.065Ω , of which about 0.03Ω is the internal resistance of the main capacitor, and the rest is the resistance of the plasma. The specific impulse is about 300 seconds on the average so that the exhaust velocity u_f is about 3000 meters per second.

Since the resistance $R \sim \frac{1}{\sigma l}$ and permeability $\mu = 4 \times 10^{-7} \text{ kg} \cdot \text{m}/\text{coul}^2$, it is found using equation 2-2 that $R_m \sim 0.05$ and $\eta \sim 1\%$. This is a low efficiency, low magnetic Reynold's number device. Also, the impulse bit $I \sim 1.8 \times 10^{-5} \text{ nt-sec} \cong 4 \mu\text{lb-sec}$ from equation 2-3b. The results of this order of magnitude analysis are low since, in reality, $\eta \cong 2\%$ and $I \cong 6.5 \mu\text{lb-sec}$.

In the previous section it was mentioned that the important parameters were $\langle dL/dx \rangle$ and $\langle R \rangle$, and that to increase the performance the former must be increased or the latter decreased.

Decreasing circuit resistance means decreasing capacitor resistance or decreasing the resistance of the plasma. The first is very difficult due to the restrictions on the

capacitor's performance characteristics (size, weight, lifetime, charging time, etc.). The second involves a detailed diagnosis of the plasma in order to find other fuels which have less resistance than teflon.

The quantity $\langle dL/dx \rangle$ can be increased in a number of different ways. One method is to change the current path in the circuit to increase the self-induced magnetic field and hence the Lorentz force on the plasma. Another way is to concentrate the magnetic field lines in the interelectrode gap using a yoke. These will be discussed subsequently in Chapter 4.

3. Thrust Balance

A. Generalities and Principle of Operation

The impulse bit of the thruster under study is very small, and it is necessary to have a measurement system which is accurate to within a few per cent and, at the same time, insensitive to random vibrations. A scheme which combines these two features at low cost involves hanging the thruster on a pendulum inside a bell jar. By evacuating the bell jar and firing the thruster once per period at the bottom of the pendulum's swing, the impulse bit can be determined from the change in amplitude. From this and measurement of the mass of teflon ablated, the specific impulse and efficiency can be calculated.

The entire system (shown in Figure 3) has several components. These subsystems have been put into three groups: (1) the pendulum, (2) the triggering and power circuits, and (3) the vacuum system. Each of these is discussed in detail in the next three sections.

B. Pendulum

The most critical part of the apparatus is the pendulum (shown in Figures 4 and 5). The top is a 1-3/4"x1-1/2"x1-1/2" brass block. Into two opposite sides of this block are pressed two hardened steel "v"-shaped knife edges. From the bottom of the block extends a two-piece, adjustable-length shaft. It consists of a 5/8" diameter, 5" long hollow brass rod into

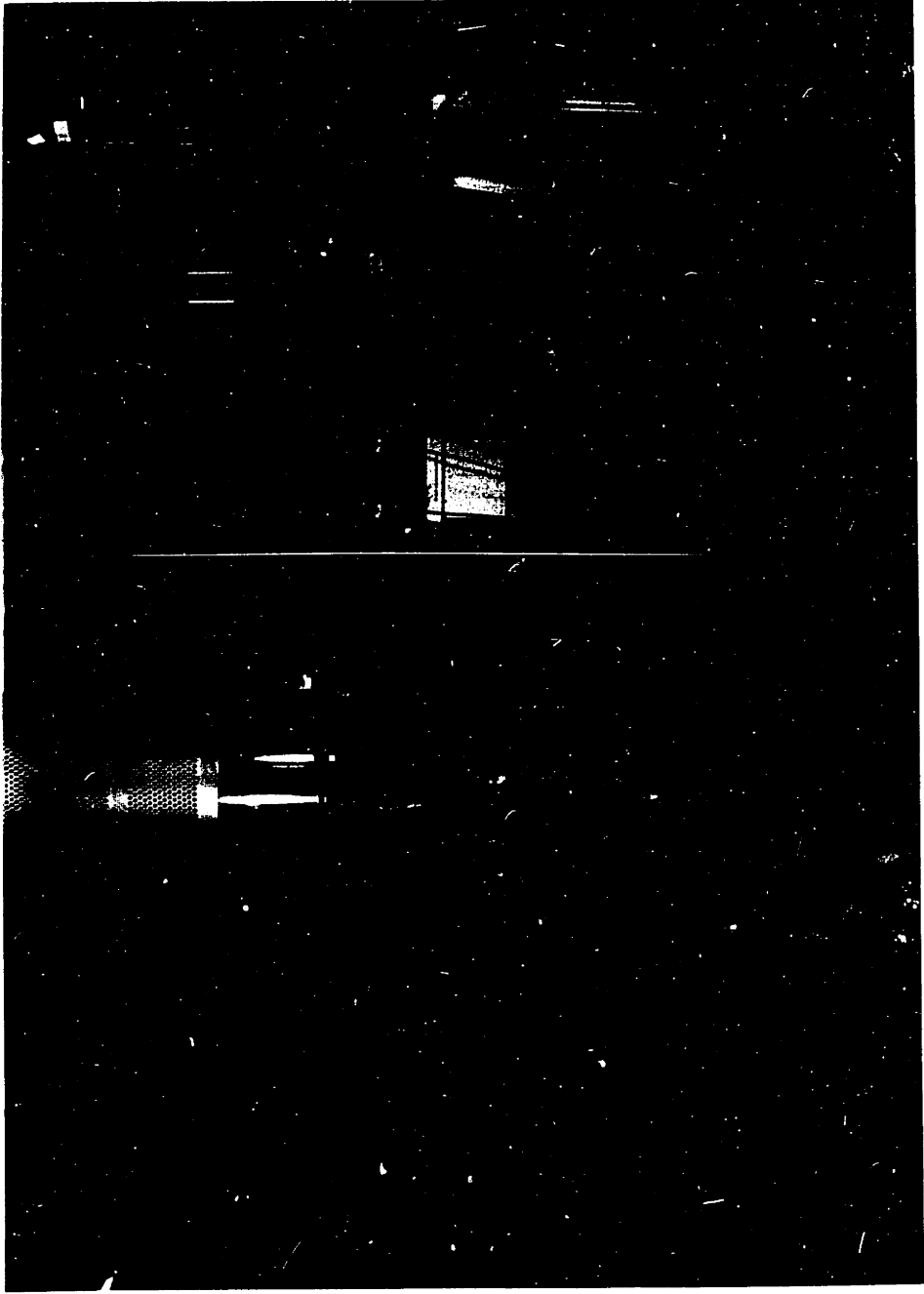


Figure 3. PHOTOGRAPH OF EXPERIMENTAL APPARATUS

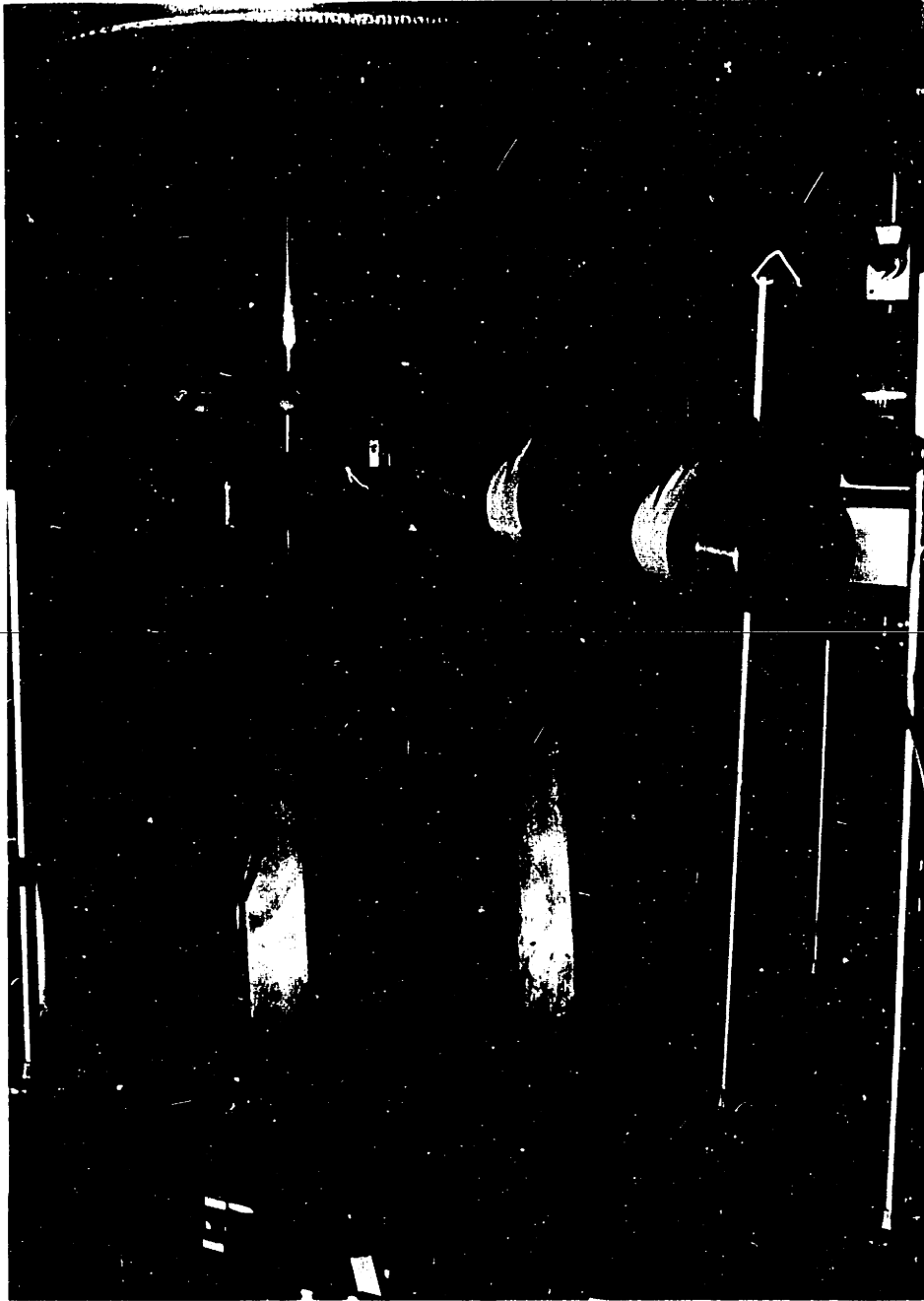


Figure 4. PHOTOGRAPH OF PENDULUM, SUPPORT STAND, AND LASER

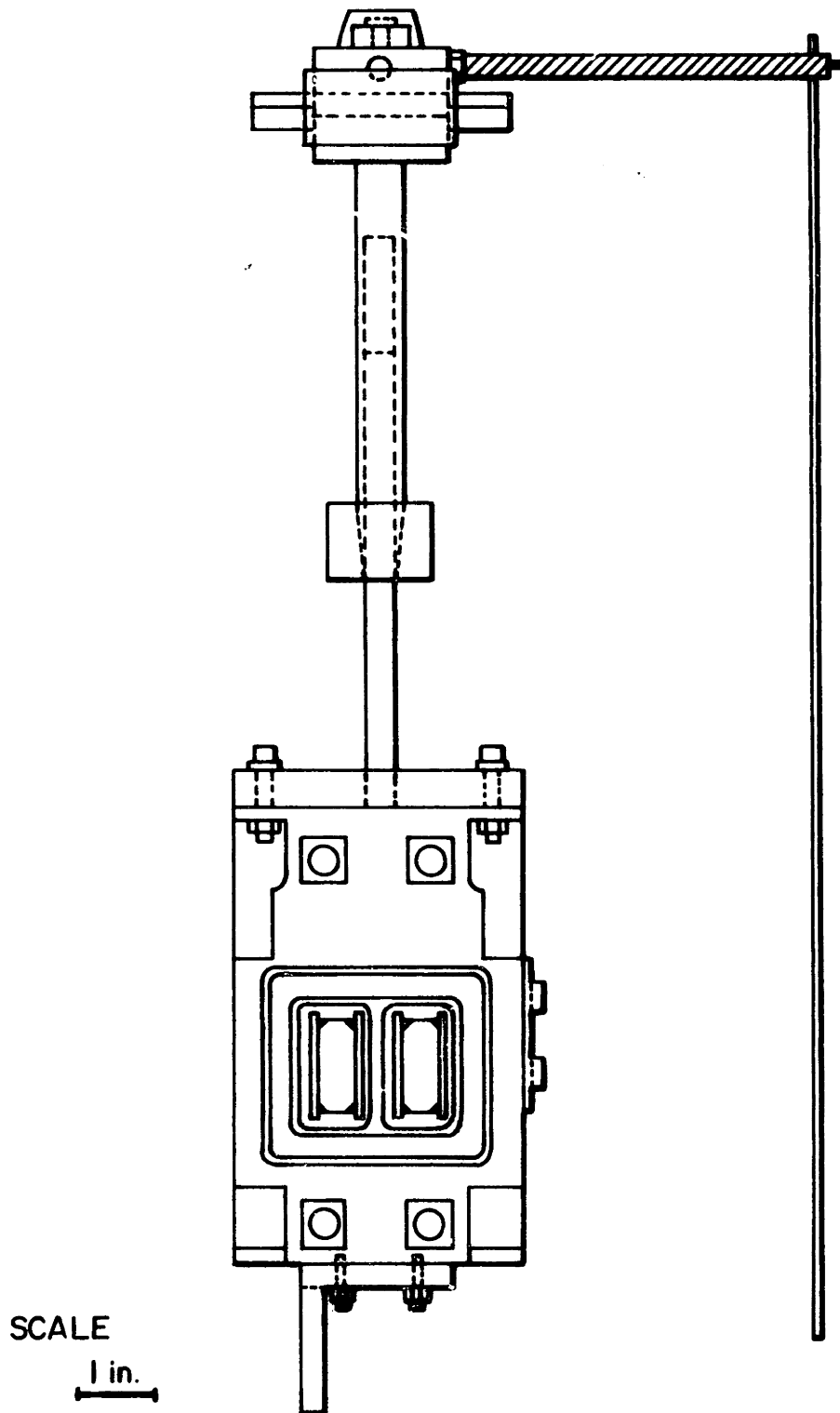


FIGURE 5. SCALE DRAWING OF PENDULUM (REAR VIEW)

which slides a 3/8" diameter, 6" long aluminum rod. (The end of the brass rod was threaded and fitted with a tightening nut.) This arrangement made possible changes in the period of the pendulum. The thruster was bolted onto a 3/8" thick aluminum plate mounted on the end of the aluminum rod.

A 9" length of aluminum angle with a 1/4" wide slit in the center of one of its legs was bolted to the bottom of the thruster. This permitted a beam of light to shine through it onto a photocell only at the bottom of each swing.

Pieces of aluminum angle and channel were welded together to provide a rigid stand for the pendulum to rest on. The most important part of this support is the two hardened steel grooves on which the knife edges rest. Initially, "v"-shaped grooves were used, but these caused very high damping due to friction. Flat pieces of hardened steel reduced damping by a factor of two, but the pendulum had a tendency to "walk." Narrow, rounded grooves, which combined the feature of small contact area between knife edge and groove with the prevention of pendulum sliding, further reduced damping to an acceptable level. In a vacuum of 2×10^{-6} torr (mm Hg), damping times of up to 13 hours were achieved with these rounded grooves for initial deflections of 5° from equilibrium.

There were four leads which connected the thruster to the external circuitry: one carrying about 10 ma at 1360 v., one carrying about 5 ma at 500 v., and two for the 6-volt triggering pulses. The critical connection was from the contact strip mounted on top of the support frame to the one

mounted on top of the pendulum. Two mil (0.002" diameter) tungsten wires were used for these leads. This was thick enough to carry the current but thin enough not to affect pendulum damping time. The four wires were separated by at least 1/4", so that in the 10^{-6} torr pressure range, arcing did not occur.

It was observed that damping time was strongly influenced by three factors: (1) pendulum amplitude, (2) bell jar pressure, and (3) pendulum center of mass. In the large amplitude range (i.e., deflections from rest of over $6\frac{1}{2}^{\circ}$), damping was higher than at lower amplitude. Consequently, all runs were made at deflection angles of less than $5\frac{1}{2}^{\circ}$. It was also found that damping was proportional to bell jar pressure. Accurate damping data could not be recorded until pressure was within the 10^{-6} torr range. Pendulum damping was also significantly affected by changes in the center of mass of the pendulum. It was necessary before each run to insure that the pendulum in its equilibrium position (i.e., rest position) hung vertically.

This thrust balance is potentially a very accurate measuring system, as long as a precise method of amplitude measurement is used. For the first two runs, a 42 cm long, 1/16" diameter aluminum pointer was used. This pointer was mounted on a brass rod which extended from one side of the brass block. With it, maximum displacements of about 4 cm could be measured to within about 5%. This large error arose from the fact that the pointer was mounted inside the

bell jar so that each end of the swing had to be determined and the value read simultaneously.

For greater precision it was necessary to separate the acts of finding the maximum position on a calibrated stick and reading the value at this position. Also, it was desirable to increase the scale of the pointer displacement to further increase the accuracy of reading it. This was accomplished by using a laser and mirror arrangement. A first surface mirror was mounted on the "nozzle side" of the brass block at the axis of rotation. A helium-neon laser (University Lab Model 240) was used for the concentrated light source to shine through the bell jar onto the mirror and be reflected onto a meter stick which was at a distance of about 8 feet. The total error in deflection angle measurement was 0.5% with this arrangement (see Appendix for detailed error analysis).

C. Triggering and Power Circuits

To trigger the thruster at the right time, an electric circuit was needed which would supply a 6-volt pulse of 1 to 10 millisecond duration at the bottom of every other swing (i.e., once per period). Since the bottom of the swing is the point of maximum velocity, it is the most efficient point for the impulsive addition of energy. Another requirement of the circuit was the ability to fire one side or the other or both sides alternately with no more than a 10 ms delay. Also, the system must not interfere with the pendulum's

motion.

To meet these requirements, a light and photocell arrangement was used. An iodine lamp focused by a convex lens was used for the high intensity light source. The slit in the aluminum angle mounted on the bottom of the thruster allowed the light to strike the photocell only at the bottom of each swing. A variable-sized aperture controlled the amount of light which reached the photocell.

A series of three relays and a 12-position stepper switch were used to provide the proper logic. This circuit (shown in Figure 6) gave a 6-volt pulse with only a 10 ms delay, and operated in the following way. When the light shined on the photocell, its resistance decreased and this increased the available voltage from a 12-volt battery sufficiently to close two relays in series with it. One relay (Iron Fireman R423-2-AB-1.1K) caused a 6-volt pulse to be sent to the stepper switch and on to the thruster on every other step. The other relay (Sigma 5RJ 2500-SIL) cut the 6-volt pulse short (to about 1 ms) by causing the stepper switch to step once. When the light was off the photocell, the relays opened and the Sigma relay caused a counter to move once. The mode selector switch, connected to 6 of the 12 stepper switch contacts, determined the side of the thruster to be fired. The manual single-step switch was used to change the thruster from direct to retro fire or vice versa.

The two power circuits provided the 1360 volts and

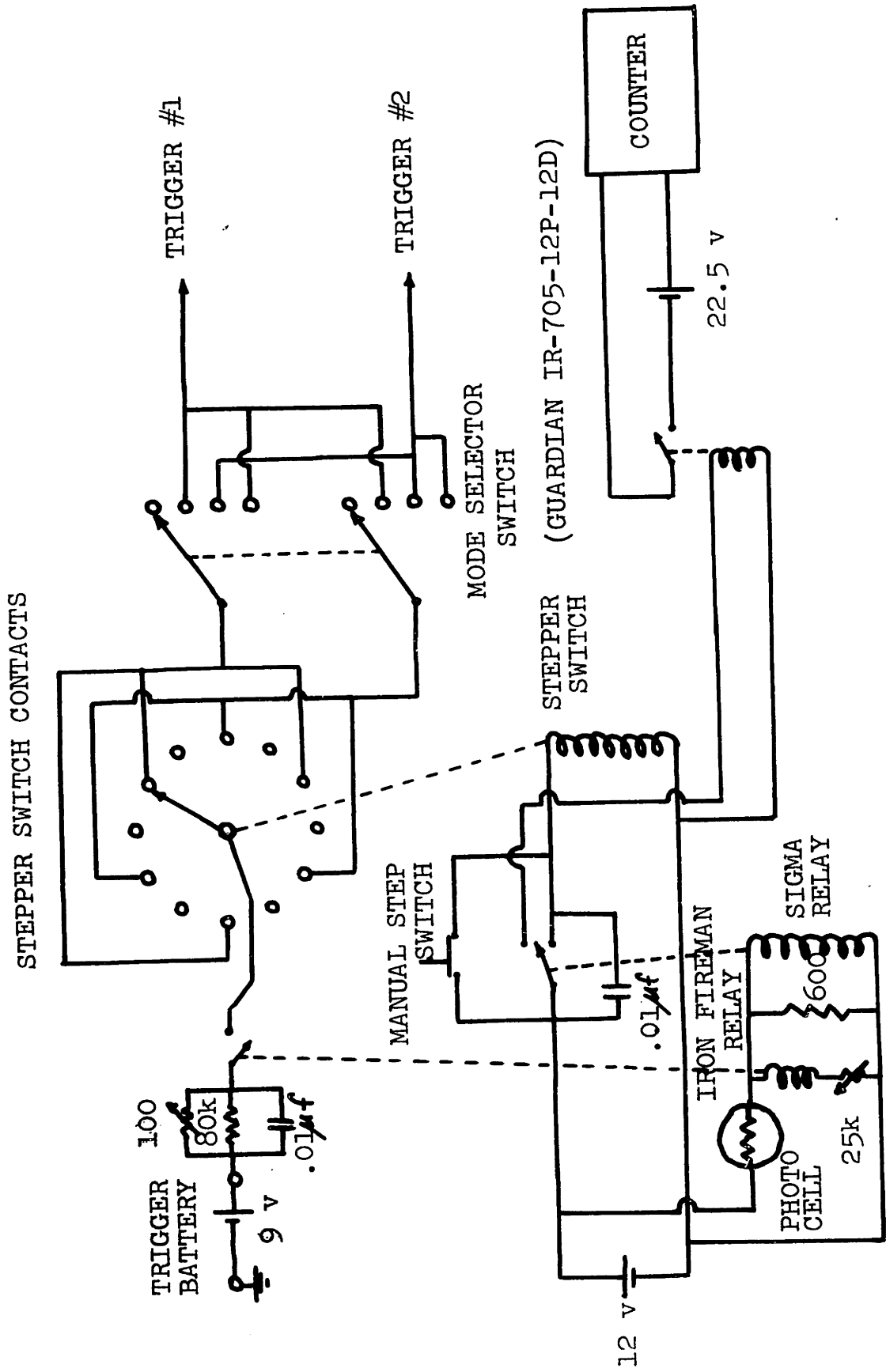


Figure 6. TRIGGERING CIRCUIT DIAGRAM

500 volts to charge the two capacitors inside the thruster between firings. For the main capacitor, a 2 kv Sorenson power supply (Model 5002-10) was used. For the smaller capacitor, a 1.2 kv Kepco power supply (Model 1220) was used. A Brush Mark 240 two-channel paper recorder was used to monitor the two power circuits to insure that both capacitors were fully charged at each period throughout the run.

D. Vacuum System

The vacuum system used for all experimental runs was the NRC Model 3316 Vacuum Coater. The primary parts of the system are a 17" diameter, 30" high bell jar which is evacuated by a mechanical pump (Welch Model 10 CFM 1376 BG), a diffusion pump (NRC Model NHS6), and a Model 0315 6" cryo-baffle (using liquid nitrogen). Vacuums in the 10^{-7} torr pressure range can be achieved with this system. It was observed that a pressure of about 2×10^{-6} torr was low enough to prevent shorting between the electrodes due to carbon deposits during the 2 to 3 hour firing times.

It was necessary to insure that the 2×10^{-6} torr pressure was low enough to prevent two adverse effects from occurring. These two problems which have invalidated the results of many electric propulsion experiments can be stated as follows: (1) What is the ratio of fuel molecules to foreign gas molecules during and after each shot?, (2) How many foreign gas molecules are adsorbed on the surface of the teflon block between shots? Question (1) arises from the

phenomenon of entrainment and acceleration of foreign gas particles in experiments with high self-induced and applied magnetic fields. Question (2) is significant when a large number of gas molecules is adsorbed on the surface of the fuel element so that the actual fuel is not pure teflon but a mixture of teflon and foreign gas molecules.

To answer question (1), we can make the following estimate: the pressure is 2×10^{-6} torr (i.e., 2.63×10^{-9} atm). Since the bell jar is at room temperature and the volume of the discharge is about 1 cm^3 , then the number of gas molecules in this volume is about 7×10^{10} . The mass of teflon expended per shot is 10^{-5} gram, so that $n_{\text{teflon}} \sim 3.6 \times 10^{17}$. Taking the ratio gives $n_{\text{teflon}}/n_{\text{gas}} \sim 5 \times 10^6$, hence entrainment of gas particles is negligible.

The worst possible case is taken to answer question (2) so that the result will be conservative. The number of gas molecules impinging on the fuel element is given by the following:

$$N = n_{\text{gas}} \frac{c}{4} S t$$

Here c = the average speed of the gas molecules $\sim 4,000 \text{ cm/s}$,
 S = the surface area of the face of the fuel element $\sim 3 \text{ cm}^2$,
 $n_{\text{gas}} \sim 7 \times 10^{10}$ (from question (1)), and t = the time between shots ~ 1 second. With these values N is about 2.1×10^{14} , and, taking this as an upper limit for the number of gas molecules adsorbed, the ratio $n_{\text{teflon}}/N \sim 1700$. Consequently,

this effect is negligible.

E. Equation of Motion

Now that the pendulum has been described conceptually and physically, it remains to be described mathematically.

The equation of motion is as follows:

$$\frac{d^2\alpha}{dt^2} + 2\nu \frac{d\alpha}{dt} + \omega_c^2 \alpha = \frac{F}{mg} \frac{l'}{l} \omega_c^2 \quad (3-1)$$

The symbols in this equation are defined in the following way:

α = deflection angle from rest position (in radians)

t = time

$1/\nu$ = damping time of pendulum

$\omega_c = \omega / (1 - \nu^2/\omega^2)$

ω = frequency of pendulum = $2\pi/T$

T = period

m = pendulum mass

g = acceleration due to gravity = 9.81 m/s^2

l' = distance from axis of rotation to center of thrust

l = distance from axis of rotation to center of mass
of pendulum.

The second term on the left-hand side of equation 3-1 (i.e., the damping term) assumes that the damping of the pendulum is proportional to its velocity. This corresponds to an approximation which retains the lowest order nonvanishing term in a Taylor series expansion. The validity of this approximation was checked experimentally by plotting amplitude versus time on semilog paper. The result was a straight

line, thus establishing the validity of the form of the damping term.

Now a typical firing, say the Nth firing, will be considered. This particular period starts with the pendulum at deflection angle α_{N-1} . Near the bottom of the swing the thruster starts firing at α_i and finishes at α_f . Then the pendulum completes this swing, and swings back to an angle α_N to complete the cycle.

Since the thrust is impulsive ($3 \mu\text{S}$), it is valid to say that $(t_f - t_i) \ll T$ and that $(\alpha_f - \alpha_i) \ll \alpha_{N-1}$, hence $\alpha_f \approx \alpha_i$. Integrating the equation over time from t_i to t_f and noticing that impulse bit $I = \int_{t_i}^{t_f} F dt$, we obtain $(\dot{\alpha}_f - \dot{\alpha}_i) + \omega_c^2 \int_{t_i}^{t_f} \alpha dt = \frac{I}{mg l} \omega_c^2$. But $\alpha \approx 0$ so that $\int_{t_i}^{t_f} \alpha dt \approx 0$ and the equation becomes:

$$\dot{\alpha}_f - \dot{\alpha}_i = -\frac{I}{mg l} \omega_c^2 \quad (3-2)$$

The negative sign arises due to the sign convention that direct fire is positive and retro fire is negative. For zero thrust, the solution of equation 3-1 is of the form

$$\alpha = \alpha_0 e^{-\nu t} \cos \omega t. \quad \text{Hence, before the Nth firing,}$$

$$\alpha = \alpha_{N-1} e^{-\nu t} \cos \omega t \quad \text{and, at } t = t_i:$$

$$\alpha = \alpha_i = \alpha_{N-1} e^{-\nu t_i} \cos \omega t_i$$

$$\dot{\alpha} = \dot{\alpha}_i = \alpha_{N-1} e^{-\nu t_i} (-\nu \cos \omega t_i - \omega \sin \omega t_i)$$

Since the thrust is impulsive,

$$t_i \cong \frac{T}{f} \left(\frac{1}{f} \right) = \frac{\pi}{2\omega}$$

After firing, $\alpha = \alpha_N e^{-\nu(t-T)} \cos \omega t$. This form is necessary because the impulsive thrust has added energy to the pendulum and has thus changed its amplitude. This means that the origin (i.e., $t = 0$) has been changed so that α equals α_N at $t = T = 2\pi/\omega$. Proceeding in the same manner as for α_1 and noticing that $t_f \cong t_i \cong \pi/2\omega$, equation 3-2 takes the following form:

$$\dot{\alpha}_f - \dot{\alpha}_i = -\omega \alpha_N e^{3\pi\nu/2\omega} + \omega \alpha_{N-1} e^{-\pi\nu/2\omega} = \frac{I}{mg} \frac{l'}{l} \omega_c^2$$

or equivalently

$$\alpha_N = \alpha_{N-1} e^{-2\pi\nu/\omega} + \frac{I}{mg} \frac{l'}{l} \frac{\omega_c^2}{\omega} e^{-3\pi\nu/2\omega}$$

This is the expression for the Nth shot. It can be written for pulses N-1, N-2, N-3, etc., down to $\alpha_1 = \alpha_0 e^{-2\pi\nu/\omega}$. By successively eliminating α_{N-1} , α_{N-2} , etc., down to α_1 from the expression for α_N , we are led to

$$\alpha_N - \alpha_0 = K(1 + x + x^2 + \dots + x^{N-1}) - \alpha_0(1 - x^N)$$

where $K = \frac{I}{mg} \frac{l'}{l} \frac{\omega_c^2}{\omega} e^{-3\pi\nu/2\omega}$ and $x = e^{-2\pi\nu/\omega} = e^{-\nu T}$.

Summing the finite series in x further simplifies the equation:

$$\alpha_N - \alpha_0 = \frac{I}{mg} \frac{l'}{l} \frac{\omega_c^2}{\omega} \frac{1 - e^{-(N-1)\nu T}}{1 - e^{-\nu T}} - \alpha_0(1 - e^{-N\nu T}) \quad (3-3)$$

In all the runs made, the period T was about 1 second and damping time $1/\nu$ was about 10 hours. Also, the number of shots N was always typically greater than 5000. Hence

$\nu T \ll 1$ and $N \cong N-1$. As a result of these two very good approximations, it is observed that $\omega_c \cong \omega$ and $e^{-\nu T} \cong 1 - \nu T$. With these simplifications equation 3-3 becomes:

$$\alpha_N - \alpha_0 = \left(\frac{I}{mg} \frac{l'}{l} \frac{2\pi}{\nu T^2} - \alpha_0 \right) (1 - e^{-N\nu T}) \quad (3-4)$$

For convenience, an angle α_∞ is defined:

$$\alpha_\infty = \frac{I}{mg} \frac{l'}{l} \frac{2\pi}{\nu T^2} \quad (3-5)$$

Rewriting equation 3-4 gives the form:

$$\alpha_N - \alpha_0 = (\alpha_\infty - \alpha_0) (1 - e^{-N\nu T}) \quad (3-6)$$

It is noticed that for zero thrust, $I = 0$ and $\alpha_\infty = 0$ so that equation 3-4 is as follows for this case:

$$\alpha_N - \alpha_0 = -\alpha_0 (1 - e^{-N\nu T}) \quad (3-7)$$

The exponential can be eliminated by dividing equation 3-6 by equation 3-7. Also, by definition, $\alpha_{N_0} = \alpha_0 e^{-\nu t}$.

$$\alpha_\infty = \frac{\alpha_N - \alpha_0 e^{-\nu t}}{1 - e^{-\nu t}} \quad (3-8)$$

Equations 3-8 and 3-5 are the ones used for reducing the data. The quantity α_∞ in these two equations represents the asymptotic value (as $t \rightarrow \infty$) of α_N , the deflection angle of the pendulum, and should be constant.

F. Data Reduction

There are four main steps in reducing the data for each run. They involve successively calculating: (1) α_N versus t , (2) damping time $1/\nu$, (3) α_∞ , and (4) I , I_{sp} , and η .

Data points are taken by reading the top of the swing of a laser dot on a meter stick at various times during a run. Before firing the thruster, at least one hour of damping data was taken for every run. Also, the thruster was pulsed for at least one hour in direct fire and one hour in retro fire (a plot of meter stick reading versus time for a typical run is shown in Figure 7). The angle α_N was then determined by subtracting the rest position reading from each meter stick reading during the run, and this was divided by twice the distance from the mirror to the meter stick.

Damping time $1/\nu$ was then calculated in one of the following two ways. The first method involved plotting α_N versus t for the damping data part of the run on semi-log paper (shown in Figure 8). Since ν is constant, it could be calculated from the slope. The other method was quicker and made use of the linear plot of readings versus time. Since the firing time was much less than $1/\nu$, the lines for direct and retro fire were approximately straight. If α_0 and α'_0 are the angles for the start of direct and retro fire respectively, and if S and S' are the slopes of the

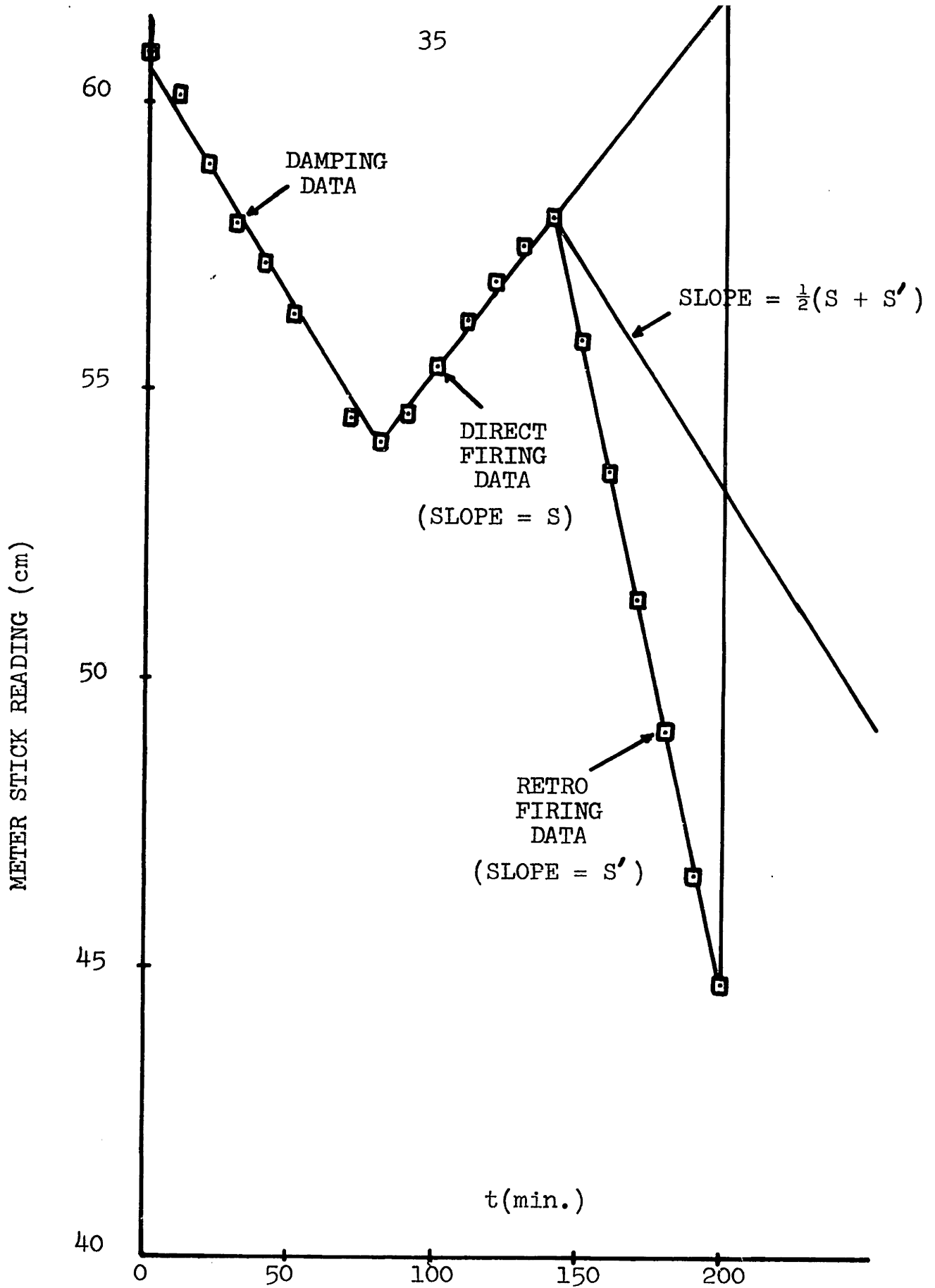


Figure 7. METER STICK READING VERSUS TIME FOR RUN #28

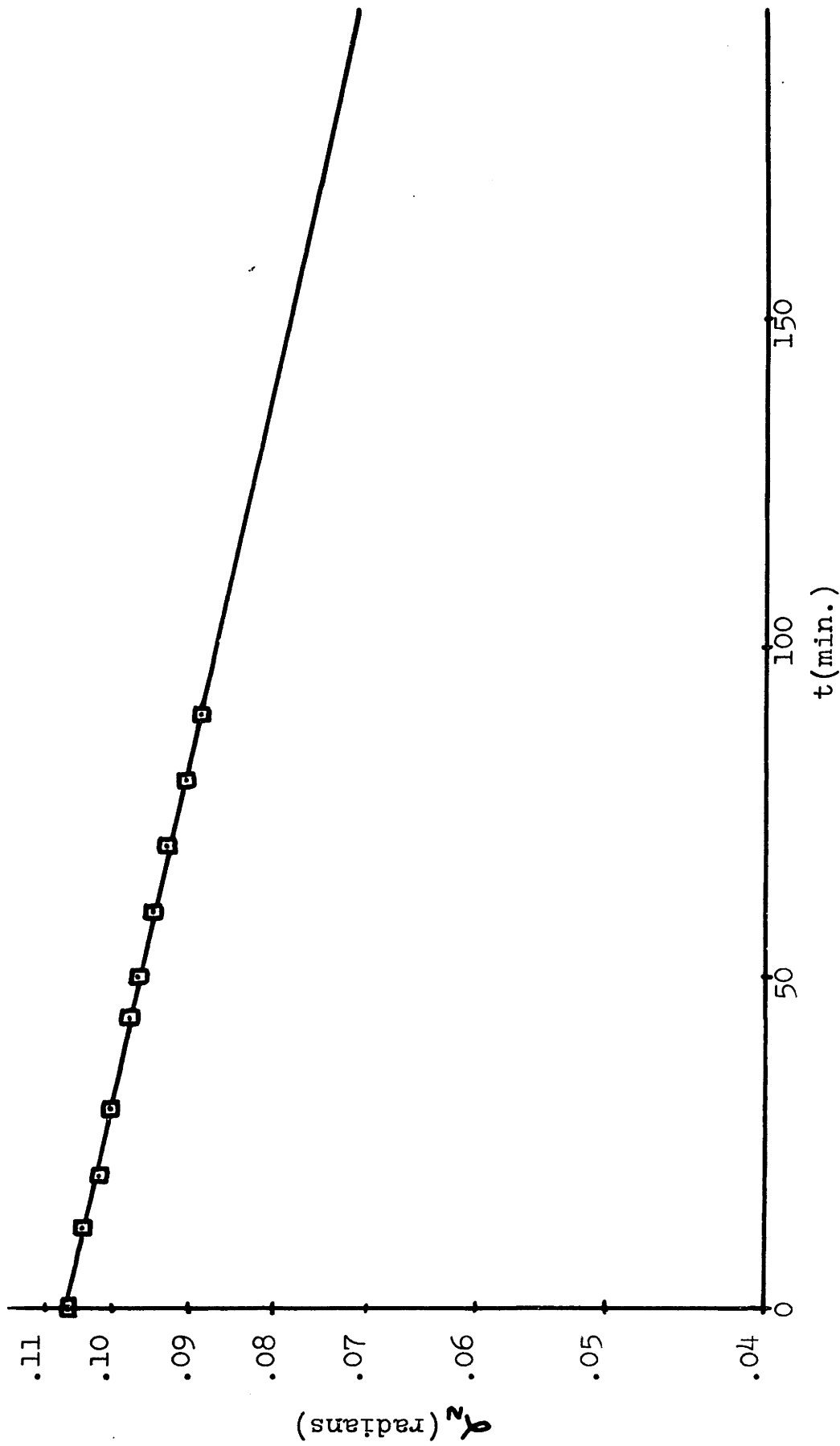


Figure 8. PLOT OF α_n VERSUS TIME FOR DAMPING DATA OF RUN #23

α_N versus t lines for both direct and retro fire, then

$$\frac{1}{\nu} = - \frac{\alpha_0 + \alpha'_0}{S + S'} \quad (3-9)$$

This latter method was the one used in most of the runs for calculating $1/\nu$, but both methods can be as much as 10% off. An error of this magnitude causes a 5% difference in α_0 for direct and retro fire. The angle α_0 was calculated separately for each point during direct and retro fire. Then it was plotted versus t on linear graph paper (as shown in Figure 9) and the average value was taken for both firing modes (note that α_0 is negative for retro fire). The first point recorded for both modes at $t = 10$ minutes usually gave an inaccurate α_0 because the numerator ($\alpha_N - \alpha_0 e^{-\nu t}$) and denominator ($1 - e^{-\nu t}$) were so small. For $t = 20$ minutes on up, the problem did not arise. By taking the average of the two values obtained for the two firing modes, the error (due to the error in $1/\nu$) cancelled and an accurate value of α_0 was obtained (see the error analysis in the Appendix for details).

Then the impulse bit was computed using equation 3-5. The number of shots N for each run was determined from the counter in the triggering circuit. In all but the first two runs, the teflon fuel elements could be removed and weighed before and after each run to determine the change in propellant mass Δm . Specific impulse was computed from I , N , and

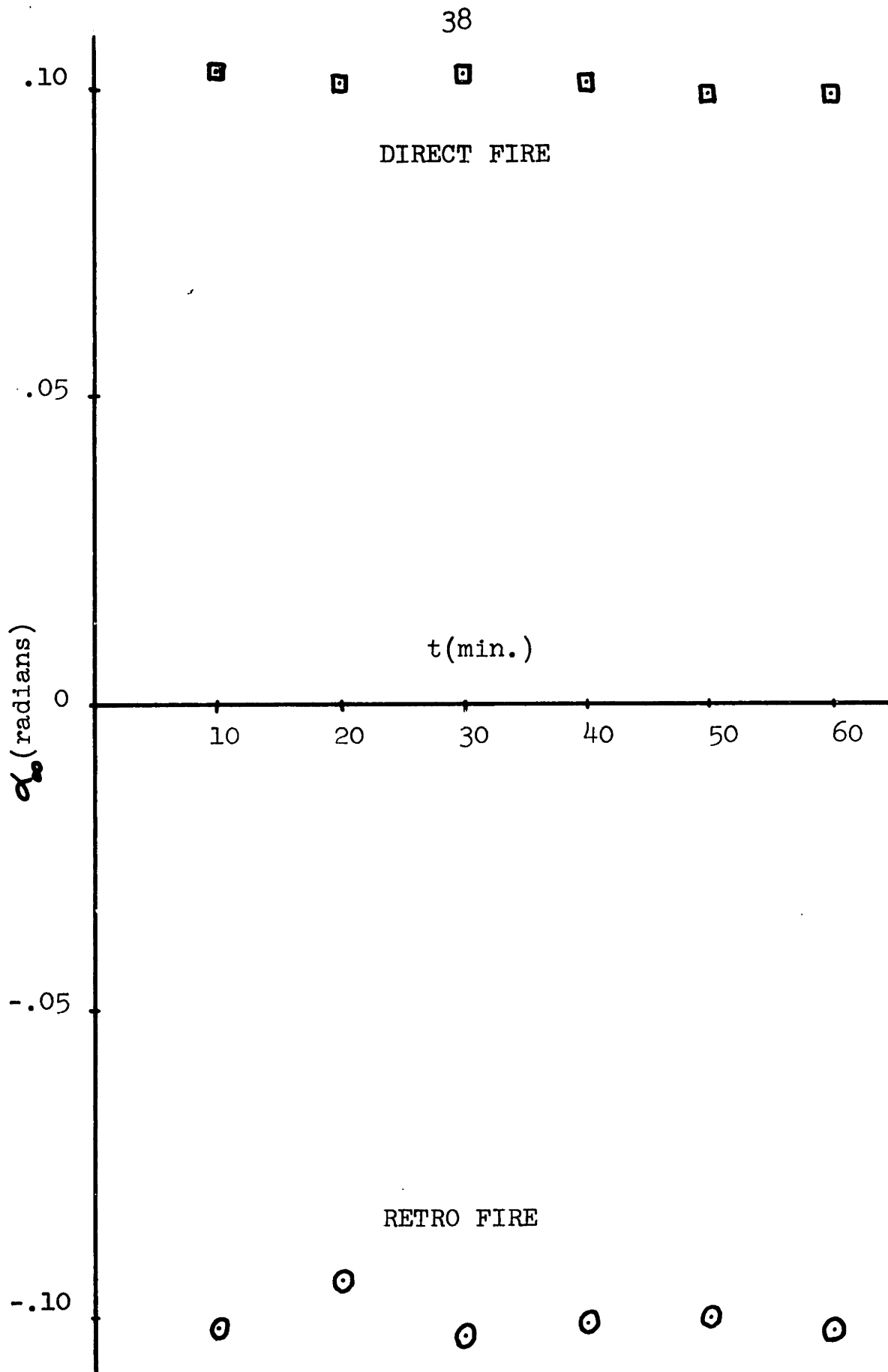


Figure 9. α_0 VERSUS TIME FOR RUN #23

Δm using the formula:

$$I_{sp} = \frac{\text{impulse bit}}{\text{weight of propellant expended/shot}} = \frac{I}{\frac{\Delta m}{N} g} \quad (3-10)$$

Efficiency was calculated using equation 2-3b.

This method of data reduction gives a total error in I of less than 2% and in I_{sp} of less than 3%.

4. Experiments

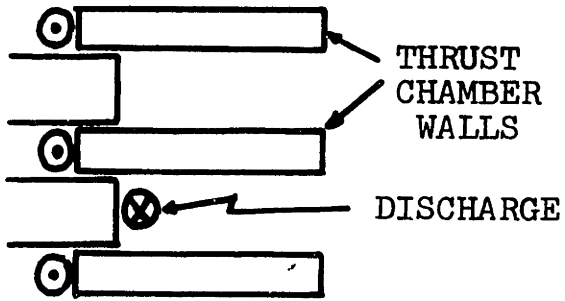
A. Generalities

On the basis of the slug model, several possible methods of improving the performance of the thruster were mentioned in Chapter 2. This particular investigation was concerned with increasing the quantity $\langle dL/dx \rangle$ by changing the current path in the main capacitor circuit.

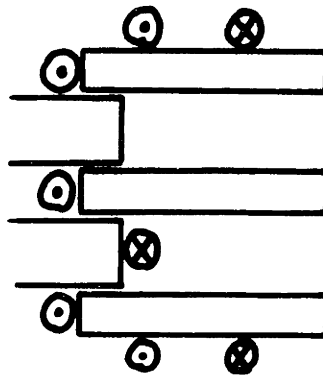
Three different groups of experiments were conducted to accomplish this. One group involved electrically insulating one side of the thruster from the other in order to make the geometry symmetric for a more symmetric force on the discharge. The use of a yoke and current loops to increase the self-induced magnetic field was examined in the other two groups. By increasing the self-field, the Lorentz force on the plasma is increased and accelerates the plasma to a higher exhaust velocity.

B. Divided Thruster

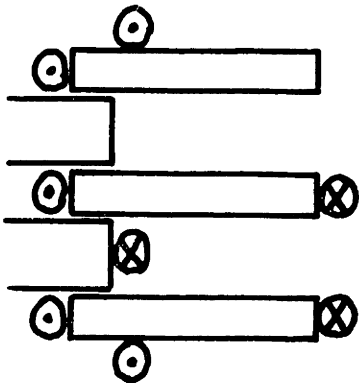
The LES-6 microthruster has three current fingers which carry the current from the main capacitor to the bottom electrode of each thrust chamber (see Figure 10a). The thruster can only be fired one side at a time, hence, the outermost current finger on the opposite side exerts a side-ward force on the discharge. Since the current in the discharge exerts a repulsive force on the current in the three fingers, the current in this outermost finger tends to a higher value which accentuates the asymmetry. To try to



a. NORMAL CONFIGURATION (N)

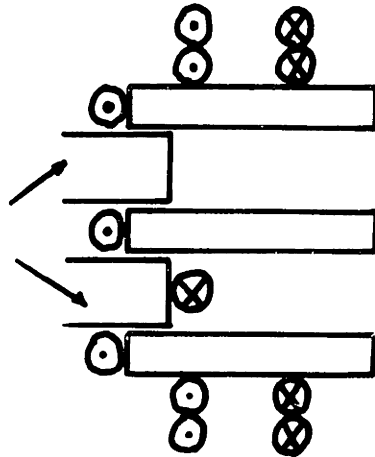


b. TWO SINGLE LOOPS (+2)

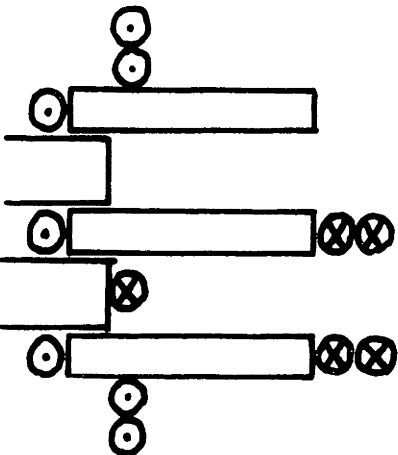


c. TWO SINGLE EXTENDED LOOPS (+X2)

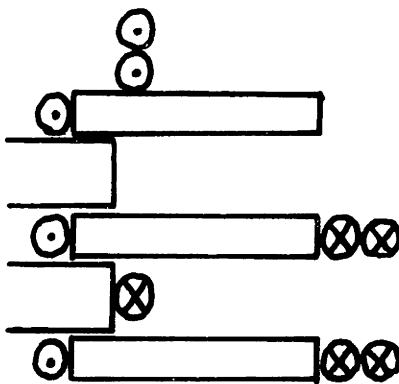
TEFLON FUEL ELEMENTS



d. TWO DOUBLE LOOPS (+4)



e. TWO DOUBLE EXTENDED LOOPS (+X4)



f. TWO SYMMETRIC DOUBLE EXTENDED LOOPS (+X4s)

Figure 10. SCHEMATIC TOP VIEWS OF THE TWO THRUST CHAMBERS WITH VARIOUS CURRENT LOOP CONFIGURATIONS

alleviate this and make each thrust chamber symmetric, the center finger was divided with a milar insulator.

Two experiments were conducted using a specially-modified, non-flight model thruster (designated RF I) to determine the change in performance. In the normal configuration (Run #19), the impulse bit was 4.43 μ lb-sec., specific impulse was 222 seconds, and efficiency was 1.2%. The same side was fired in the divided thruster (Run #18) and gave an I of 3.97 μ lb-sec., I_{sp} of 220 sec., and of 1.0%. Hence, this modification decreased, rather than increased, the performance.

C. Yoke

In Runs #6, 10, and 20, a rectangular yoke was put on the two sides and top of the thruster chamber assembly. It was designed to concentrate the magnetic field lines produced by the circuit current.

The yoke was laminated with alternate layers of 0.001" thickness high permeability metal and insulation in order to prevent dissipation of energy from eddy currents. The metal layers had a high permeability so that there was a high tendency for the field lines to be concentrated, and they had a low hysteresis to eliminate cycling losses.

In the first experiment (Run #6), the yoke caused a small increase in performance: I from 6.23 to 6.34, I_{sp} from 274 to 285. Apparently, the field lines closed upon themselves rather than penetrating the yoke.

A possible solution was to divert the current path around the yoke to increase the penetration and increase circuit inductance. The circuit was broken with a milar insulator, and a single loop of wire was put around the yoke on each thrust chamber in series with the discharge so that the current would go around and close to the yoke. This decreased I from 6.83 to 5.40 and I_{sp} from 348 to 311 (in Run #10). When two double loops were put around the yoke (in Run #20), performance was further decreased to an I of 4.08 and an I_{sp} of 305.

Hence, loops around the yoke caused a decrease in performance which worsened when the number of loops was increased. This may be due to the fact that these configurations increased the circuit inductance. As L increases, the quantity $4L/R$ increases relative to the circuit capacitance C . In the normal configuration, the main capacitor circuit exhibits a damped oscillatory current behavior with time during the discharge (i.e., $C < 4L/R$).² When L is increased with C and R constant, the amount of ringing increases and may increase to the point where the capacitor has not fully discharged its energy before the discharge has moved out of the electrode gap. This would explain why more loops around the yoke further decreased the performance.

Here a remark should be made about the increase in performance with the normal configuration from Run #6 to Run #10. The reason for the increase was that a new main

capacitor had been put in the flight model thruster being tested. This new capacitor had a lower internal resistance (i.e., lower $\langle R \rangle$) which caused an increase in I from 6.23 to 6.83 and in I_{sp} from 274 to 348.

D. Current Loops

In the configurations which caused the greatest changes in thruster performance, loops of wire were used to change the current path in the main capacitor circuit. The circuit was broken with a milar insulator, and the current was diverted through loops along each side of the thrust chamber assembly.

The first configuration investigated had two single loops on each side of the thrust chamber assembly (shown in Figure 10b). Three runs were made with this modification, all with the same flight model microthruster but the first with the older capacitor, and each run gave a different result. In Run #7, the impulse bit was decreased from 6.23 to 4.74, and the specific impulse was increased from 274 to 283. The same configuration was used in Run #25, but with the new capacitor (i.e., capacitor #2), and I was decreased from 6.83 to 4.04, and I_{sp} increased from 348 to 482. Prior to this run, the face of the fuel element had been cleaned with an automatic sander to prevent the unevenly ablated surface from affecting the results. This heated the block to a temperature high enough to change the surface by the adsorption of air molecules onto it. The run was repeated

(in Run #29) to check the results, and it was found that I was 4.58 and I_{sp} was 333. Since the efficiency for this run was 1.8%, it was a 1% decrease from that of the normal flight model with capacitor #2.

The next logical step was to extend these single loops outside the case of the thruster (as shown in Figure 10c). The I_{sp} was considerably increased (from 348 to 462), I was decreased (from 6.83 to 3.10), and η was decreased (from 2.8% to 1.7%) in Run #15. The problem with this arrangement is that the two thrust chambers are built together so that the loops were not symmetric when firing one side. As a result of this asymmetry, a strong sideward force was exerted on the plasma causing the thrust (i.e., impulse bit) to be decreased. This was evidenced by the fact that the center wall was completely covered with carbon by the end of the run, while the outer wall was only lightly coated.

With two double extended loops (see Figure 10e) in Run #21, I_{sp} was more than doubled to 934, and I was cut to 1.86 with an η of 2%, but carbonization of the center wall was so fast that the run had to be stopped after only 70 minutes of firing. To symmetrize the force on the discharge, a scheme was tried using a double extended loop on the far side and a single extended loop on the near side to the discharge (in Run #22). The carbonization was alleviated, but the performance was further decreased.

Two simple double loops (shown in Figure 10d) were tried in Run #23 to give good performance with low carbonization. The result was an I of 2.70, an I_{sp} of 562, and an η of 2% with less carbon coating of the walls than in the runs with the extended loops.

Reversing the current direction in the single loops in Run #12, in the double loops in Run #24, and in the single extended loops in Run #28 caused poorer performance in all cases. These runs were made to determine the effect of current direction on performance.

On the basis of the previous runs, double extended loops were the most promising modification provided they could be arranged symmetrically with respect to the sides of the thruster being fired. The extended part of the loops had the greatest influence on the discharge, but it was the back edge of the loops on the side closest to the discharge which was responsible for driving the discharge toward the center wall. This was corrected by using an extra wide plastic spacer to make the loops symmetric (see Figure 10f). Run #30 confirmed this by reducing the carbonization of the center wall and producing an I_{sp} of 1002, an I of 2.11, and an η of 2.5%.

In this configuration, part of the discharge attached itself to the metallic nozzle (through a small hole in the insulation) in about one shot out of every ten. Run #31 was conducted without the nozzle but with the same loop configuration as in Run #30. This modification produced an I_{sp} of 669,

an I of 1.72, and an η of 1.4%. Throughout the run, there was a high current leakage to teflon deposits on the case of the thruster, on the aluminum angle mounted on the bottom, and on the thrust chamber mouth. As in the previous run, the current appeared to complete the circuit through these deposits rather than through the discharge to the electrodes.

E. Summary of Results

The results of all the successful runs are presented in Table 1. For convenience, a system of designations has been devised for the more important runs. A number prefixed by a plus or minus sign represents the number of loops and current direction. Extended loops are designated by the letter "X" in addition to the sign and number (as in Figure 10). The letter "Y" indicates runs in which a yoke was used, and the number indicates the number of wires around it.

The runs which resulted in the greatest change in performance (i.e., configurations +2, +X2, +4, +X4, +X4s) are shown in Figure 11 on a plot of impulse bit versus specific impulse. A trend is evident from this series of runs that as specific impulse increases, impulse bit decreases with about the same efficiency ($\sim 2\%$).

There seems to be two reasons for this tradeoff between I and I_{sp} : (1) a higher exhaust velocity allows the discharge less time to ablate off teflon and, hence, reduces the mass of fuel expended per shot, (2) the use of loops of wire increases the circuit inductance which increases the

Table 1. SUMMARY OF EXPERIMENTAL RESULTS

<u>Run</u>	<u>I</u> <u>(μlb-sec.)</u>	<u>Isp</u> <u>(sec.)</u>	<u>η (%)</u>	<u>Thruster</u> <u>Model</u>	<u>Configuration</u>	<u>Designation</u>
1	5.27	Not Measured		Flight	Normal	N
2	5.20	NM		Same	Same	N
5	6.23	274	2.0	Flight but different than in Runs #1, 2	Normal	N'
6	6.34	285	2.1	Same	Yoke	Y
7	4.74	283	1.6	Same	2 single loops	+2
10	5.40	3.11	2.0	Same but with new main capacitor (#2)	Yoke with 2 single loops around it	Y2
12	5.03	314	1.9	Same	2 single loops with reversed current	-2
14	3.44	355	1.4	Same	2 extended single loops without plastic spacers*	

*Plastic spacers were used in all runs with current loops (except Run #14) to insure that the back edges of the loops were even with the face of the teflon fuel element.

Table 1. (Continued)

<u>Run</u>	<u>I</u> (<u>μlb-sec.</u>)	<u>I_{sp}</u> (<u>sec.</u>)	<u>η (%)</u>	<u>Thruster</u> <u>Model</u>	<u>Configuration</u>	<u>Designation</u>
15	3.10	462	1.7	Same	Same as Run #14, but with spacers	+X2
16	6.83	348	2.8	Same	Normal	N''
18	3.97	220	1.0	RF I	2 sides electrically separated	
19	4.43	222	1.2	Same	Normal	
20	4.08	305	1.5	Same as in Run #10	Yoke with 2 double loops around it	+Y4
21	1.86	934	2.0	Same	2 double extended loops	+X4
22	2.73	372	1.2	Same	1 double loop and 1 single loop	+X3
23	2.70	562	1.8	Same	2 double loops	+X4
24	5.23	323	2.0	Same	2 double loops with reversed current	-X4
26	4.04	482	2.3	Same	2 single loops	+2
27	4.49	261	1.4	Same	2 single extended loops with reversed current	-X2

Table 1. (Continued)

<u>Run</u>	<u>I</u> <u>(μlb-sec.)</u>	<u>Isp</u> <u>(sec.)</u>	<u>η(%)</u>	<u>Thruster</u> <u>Model</u>	<u>Configuration</u>	<u>Designation</u>
28	4.58	234	1.3	Same	Same	-X2
29	4.58	333	1.8	Same	2 single loops	+2
30	2.11	1002	2.5	Same	2 symmetric double extended loops	+X4s
31	1.72	669	1.4	Same	Same as Run #30 but without nozzle	

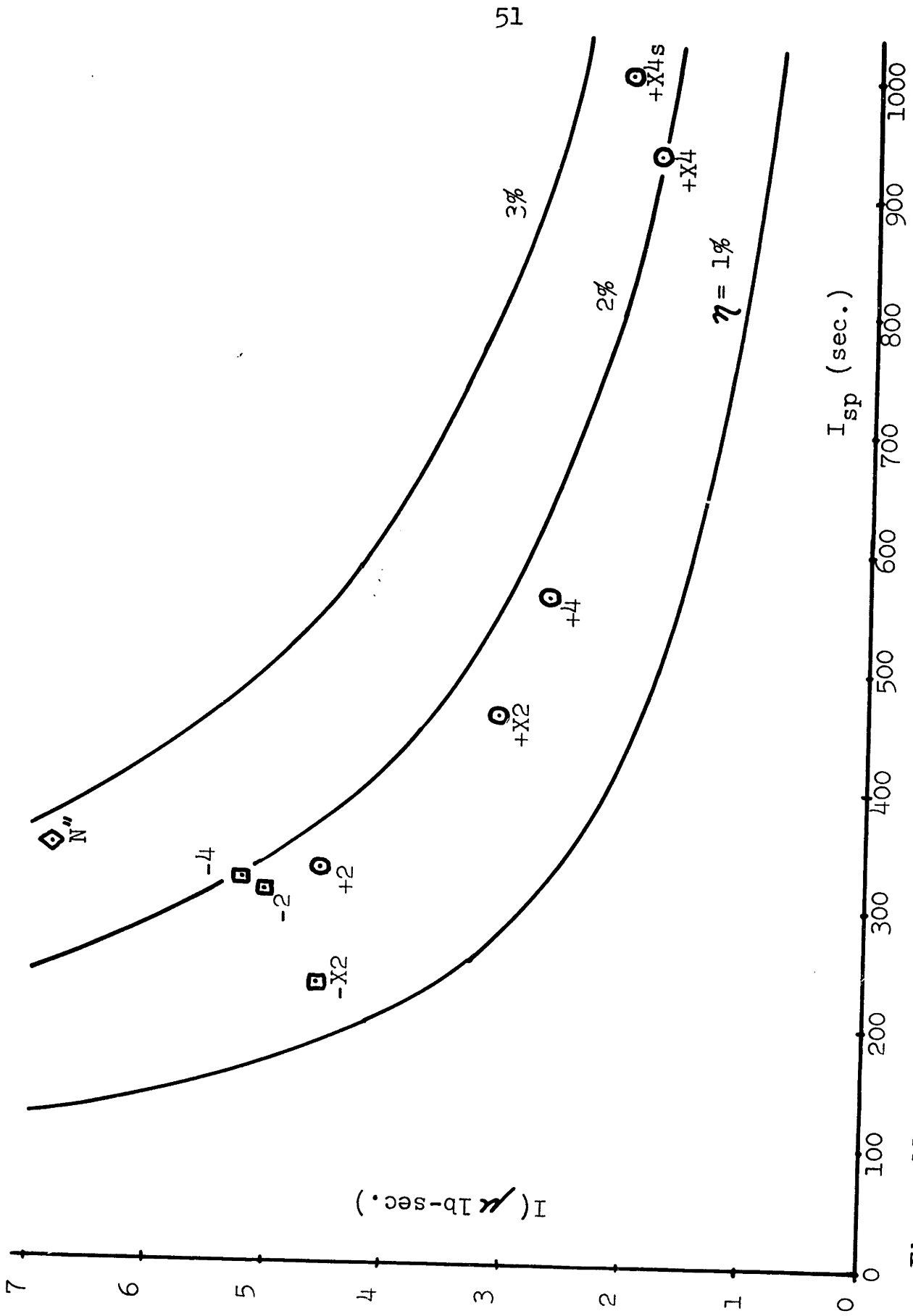


Figure 11. THRUSTER PERFORMANCE FOR VARIOUS CURRENT LOOP CONFIGURATIONS

decay time of the damped oscillatory circuit current, hence, there is less energy in the discharge at its initial position (i.e., close to the teflon block). Reason (2) is substantiated by the visual observation, mentioned in the previous section, of current leakage beyond the electrodes.

An order of magnitude analysis will now be proposed to explain this numerically. First, we will define a dimensionless variable L' which is the ratio of inductance of configuration +X4s to the normal configuration. Experimentally, the normal inductance is 4×10^{-8} henry. The +X4s inductance can be calculated by assuming that the circuit consists of two pairs of rectangular loops (one pair in parallel with the other) approximately 2" long, 1-1/2" wide, and 0.04" thick. Using these dimensions, the inductance of one loop is roughly 1.2×10^{-7} henry³, or the total is about 1.2×10^{-7} h. This means that L' is about 3. In an RLC circuit the time for a discharge is proportional to $1/L$. Hence, it is reasonable to assume that the amount of energy dissipated while the discharge is between the electrodes is $E \sim 1/u_f L$. This means that the mass expended per shot goes like $1/u_f L$, i.e.

$$m \sim \frac{1}{u_f L} \quad (4-1)$$

From equation 2-5 with $E \sim 1/u_f L$, we get the following:

$$I \sim \frac{dL}{dx} \frac{1}{u_f L} \quad (4-2)$$

Substituting equation 4-2 into equation 2-3a results in the following:

$$\eta = \frac{I u_f / 2}{E_{total}} \sim \frac{dL}{dx} \frac{1}{L} \quad (4-3)$$

But experimentally on the basis of the runs with loops, η is nearly constant. Hence, dL/dx is proportional to L and from equation 4-2:

$$I \sim \frac{1}{u_f} \quad (4-4)$$

To determine the variation of I_{sp} with L , we refer to equation 3-10:

$$I_{sp} = \frac{I}{\frac{4m}{N} g} \sim \frac{I}{\dot{m}} \sim L \quad (4-5)$$

Comparing the results of Run #30 with the normal configuration, it can be seen that: (1) η is nearly the same for both runs (2.5% and 2.8%), (2) I_{sp} is increased by about a factor of 3 from 348 to 1002 seconds and, hence, varies as L' , and (3) I is decreased by about a factor of 6.83 to 2.11 and, hence, varies as $1/u_f$.

One more calculation can be made to verify the validity of the analysis. The time for discharge of this circuit is somewhat longer than $2L_o/R_o$ or about $1.5 \mu s$ for the normal thruster and about $4.5 \mu s$ for the +4Xs. The exhaust

velocities for the normal and +X4s thrusters are 3500 m/s and 10,000 m/s respectively so that the distance to complete the discharge (which is proportional to uL) is about 0.5 cm in the former and 4.5 cm in the latter. The electrodes are about 1 cm long; hence, the current in the +X4s configuration must be completed through the nozzle (or the case) of the thruster.

5. Conclusion

Substantial changes in the performance of this pulsed solid fuel microthruster were made by changing the path of the circuit current to increase the self-induced magnetic field. Diverting the current through loops of wire on the sides of the thrust chamber assembly had the greatest effect on performance by accelerating the discharge to higher exhaust velocities.

One of the problems encountered with the modifications was the sideward force exerted on the discharge due to the asymmetry. Symmetric, extended current loops greatly increased specific impulse and reduced the sideward force. Impulse bit was decreased, however, while the overall efficiency remained about the same. This tradeoff between impulse bit and specific impulse results from two factors mentioned in the last section of Chapter 4, namely that the higher exhaust velocity reduces the mass of teflon ablated, and that the increased inductance increases the decay time to the point where less energy goes into the discharge.

The key to improving the performance of this type of thruster lies in changing the geometry in such a way as to increase the self-induced magnetic field without substantially increasing the circuit inductance. It would be interesting to try some of these loop configurations, particularly the +X⁴s, on a larger scale thruster. It would also be interesting to try two symmetric triple extended loops (i.e., +X⁶s).

APPENDIX

Error Analysis

In order to estimate the total error in thrust measurement, the error in each measured quantity will be examined. The equation for the impulse bit is as follows:

$$I = A \nu \alpha_{\infty}$$

where

$$A = mg \frac{l}{l'} \frac{T^2}{2\pi}$$

and

$$\nu \alpha_{\infty} = \nu \frac{d_N - d_0 e^{-\nu t}}{1 - e^{-\nu t}}$$

Hence

$$\frac{\Delta A}{A} = \frac{\Delta \left(mg \frac{l}{l'} \frac{T^2}{2\pi} \right)}{m \frac{l}{l'} \frac{T^2}{2\pi}} = \frac{\Delta m}{m} + \frac{\Delta l}{l} + \frac{\Delta l'}{l'} + \frac{2\Delta T}{T}$$

The pendulum mass m is about 3 kg for all the runs and could be measured to the nearest tenth of a gram. This gives an error of less than 0.003%. Error in l' is 1/32" out of about 12" or 0.25%. The length l was over 8-1/2" for all runs and the error is 1/16" or 0.7%. The period T is accurately given by dividing the total firing time Δt_f by the number of shots N . Error in Δt_f is less than 5 seconds out of 2 hours or 0.07%, and error in N is 1 shot out of at

least 6000 or 0.05% so that the maximum error in T is 0.1%.

Hence, the maximum error in the quantity A is 1%, i.e.,

$$\Delta A/A = 0.01.$$

Now the error in the quantity $\nu \alpha_{\infty}$ will be considered.

From the expression for $\nu \alpha_{\infty}$ we have:

$$\begin{aligned} \frac{\Delta(\nu \alpha_{\infty})}{\nu \alpha_{\infty}} &= \frac{\Delta \nu}{\nu} + \frac{\Delta(\alpha_N - \alpha_0 e^{-\nu t})}{\alpha_N - \alpha_0 e^{-\nu t}} - \frac{\Delta(1 - e^{-\nu t})}{1 - e^{-\nu t}} \\ &= \frac{\Delta \alpha_N + (\Delta \alpha_0) e^{-\nu t}}{\alpha_N - \alpha_0 e^{-\nu t}} + \frac{\Delta \nu}{\nu} + e^{-\nu t} (t \Delta \nu + \nu \Delta t) \left(\frac{\alpha_0}{\alpha_N - \alpha_0 e^{-\nu t}} - \frac{1}{1 - e^{-\nu t}} \right) \end{aligned}$$

Rewriting this equation gives the following:

$$\begin{aligned} \frac{\Delta(\nu \alpha_{\infty})}{\nu \alpha_{\infty}} &= \frac{\Delta \alpha_N + (\Delta \alpha_0) e^{-\nu t}}{\alpha_0 (1 - e^{-\nu t})} + \frac{\Delta t}{t} \frac{\nu t e^{-\nu t}}{1 - e^{-\nu t}} \left(\frac{\alpha_0}{\alpha_{\infty}} - 1 \right) + \frac{\Delta \nu}{\nu} \left[1 + \frac{\nu t e^{-\nu t}}{1 - e^{-\nu t}} \left(\frac{\alpha_0}{\alpha_{\infty}} - 1 \right) \right] \\ &= \frac{\Delta \alpha_N + (\Delta \alpha_0) e^{-\nu t}}{\alpha_0 (1 - e^{-\nu t})} + \frac{\Delta t}{t} \frac{\nu t e^{-\nu t}}{1 - e^{-\nu t}} \left(\frac{\alpha_0}{\alpha_{\infty}} - 1 \right) + \frac{\Delta \nu}{\nu} \left(\frac{1 - e^{-\nu t} - \nu t e^{-\nu t} + \nu t e^{-\nu t} \frac{\alpha_0}{\alpha_{\infty}}}{1 - e^{-\nu t}} \right) \end{aligned}$$

Since $1/\nu \sim 10$ hours and $t \leq 1$ hour, $\nu t \lesssim 0.1$, hence, we can expand $e^{-\nu t}$ and neglect terms higher than second order, i.e.,

$$e^{-\nu t} \cong 1 - \nu t + \frac{\nu^2 t^2}{2}$$

With this approximation, the equation simplifies to the following:

$$\frac{\Delta(\nu \alpha_{\infty})}{\nu \alpha_{\infty}} \cong \frac{\Delta \alpha_N + \Delta \alpha_0}{\nu t \alpha_{\infty}} + \frac{\Delta t}{t} \left| \frac{\alpha_0}{\alpha_{\infty}} - 1 \right| + \frac{\Delta \nu}{\nu} \left(\frac{\nu t}{2} + \frac{\alpha_0}{\alpha_{\infty}} \right)$$

Errors in α_N and α_0 arise from reading the meter stick and in measuring the distance from the mirror to the meter stick. The error in t arises from performing this reading accurately with respect to time. Data points were taken every 10 minutes to the nearest second (i.e., a 0.5% error in t), and the meter stick was read to the nearest millimeter out of a total deflection of at least 40 cm. The pendulum rest position was also measured to within one millimeter. The angles α_N and α_0 were computed by subtracting the rest position from the reading and dividing by twice the distance to the meter stick. The error of this latter distance is 1/16" out of 92", making the total error in α_N and α_0 0.25%. The quantities α_0 , α_N and α_0 are all of the same order of magnitude for each run, α_0 being at least two times larger than the other two. Hence, the first two terms on the right-hand side of the equation for $\Delta(\nu\alpha_0)/\nu\alpha_0$ are as follows:

$$\frac{1}{\nu t} \left(\frac{\Delta\alpha_N}{\alpha_0} + \frac{\Delta\alpha_0}{\alpha_0} \right) = \frac{1}{\nu t} \left(\frac{\Delta\alpha_N}{\alpha_N} \frac{\alpha_N}{\alpha_0} + \frac{\Delta\alpha_0}{\alpha_0} \frac{\alpha_0}{\alpha_0} \right) \approx 0.025$$

$$\frac{\Delta t}{t} \left| \frac{\alpha_0}{\alpha_0} - 1 \right| = 0.0025$$

Therefore
$$\frac{\Delta(\nu\alpha_0)}{\nu\alpha_0} = 0.0275 + \frac{\Delta\nu}{\nu} \left(\frac{\nu t}{2} + \frac{\alpha_0}{\alpha_0} \right)$$

The quantity $\nu t/2 = 1/20$ and $\alpha_0/\alpha_0 \approx 1/2$ so that a 10% error in ν means an additional 5-1/2% error in $\nu\alpha_0$. Hence, the

most critical parameter in the calculation of impulse bit is the damping time $1/\nu$. Using either of the two methods for calculating $1/\nu$ described in Chapter 3, the error can be as high as 10%. In the most frequently used method, this inaccuracy arises because the thrust curves are approximated as straight lines (see Figure 7). The error in the other method arises from extrapolating the damping line beyond the data points (see Figure 8).

Errors in α_N , α_0 , and t vary randomly from point to point and therefore cause a random error in the calculation of $\nu\alpha_\infty$. The error in ν , however, is the same for both direct and retro firing since it is constant throughout each run. This means that α_∞ has a different value for direct and retro firing by as much as 5%. However, the sum of α_∞ for direct firing and α_∞ for retro firing is very insensitive to an error in the damping time. Hence, this error can be eliminated by averaging in the following manner:

$$\begin{aligned} \frac{\Delta(\nu\alpha_\infty)}{\nu\alpha_\infty} &= \frac{1}{2} \left[\left(\frac{\Delta(\nu\alpha_\infty)}{\nu\alpha_\infty} \right)_{\text{direct}} + \left(\frac{\Delta(\nu\alpha_\infty)}{\nu\alpha_\infty} \right)_{\text{retro}} \right] \\ &= 0.0275 + \frac{\Delta\nu}{\nu} \left(\frac{\nu t}{2} \right) = 0.0325 \end{aligned}$$

However, this 3.25% error in $\nu\alpha_\infty$ must be divided by a factor of 5 since at least 5 points in each of retro and direct firing were used to compute α_∞ for each of these firing modes. This means that $\Delta(\nu\alpha_\infty)/\nu\alpha_\infty = 0.007$.

Hence,

$$\frac{\Delta I}{I} = \frac{\Delta A}{A} + \frac{\Delta(v\alpha_{\infty})}{v\alpha_{\infty}} = 0.017$$

and the error in impulse bit is seen to be less than 2%.

The error in specific impulse arises from inaccuracies in measuring the mass expended Δm , the number of shots N , and the impulse bit I according to the following equation:

$$\frac{\Delta I_{sp}}{I_{sp}} = \frac{\Delta m}{m} + \frac{\Delta N}{N} + \frac{\Delta I}{I}$$

The error in N is 0.05% and in I is 2%. The mass of the teflon block was measured on an analytical balance which is accurate to one ten-thousandth of a gram. Since for all runs $\Delta m \geq 0.0140$ gram, the error is less than 1%. However, for most runs $\Delta m \geq 0.05$ gram so that the error is usually less than 0.2%. Hence, the error in I_{sp} is less than 3%.

REFERENCES

1. Guman, William J., Pulsed Plasma Technology in Microthrusters, Air Force Aero Propulsion Laboratory Technical Report 68-132, Wright-Patterson AFB, Ohio, November, 1968.
2. Jahn, Robert G., Physics of Electric Propulsion, McGraw-Hill, Inc., N.Y., 1968, 266-267.
3. Henney, Keith, Radio Engineering Handbook, McGraw-Hill, Inc., N.Y., 1959, 3-17.